A method for investigating dynamic direct shear behavior of artificial jointed rocks using CNS direct shear box and Long Bar Drop Impact (LBDI) System

Hanlim Kim, Gyeongjo Min, Gyeonggyu Kim, Youngjun Kim
Jeonbuk National University, Jeonju, South Korea

Sangho Cho (corresponding author)
Jeonbuk National University, Jeonju, South Korea

Jusuk Yang, Kyungjae Yun
Agency for Defense Development, Daejeon, South Korea

ABSTRACT: Understanding the shear behavior of a discontinuity in rock masses is vital for the proper design and construction of underground structures, considering their structural stability and cost efficiency. A static-based shear behavior is generally considered for designing these structures; however, rocks often undergo dynamic loading, such as seismic, blast, and percussive loading. Various studies have reported that rocks exhibit significantly different mechanical behaviors under dynamic loading, and frictional behavior may also exhibit different behaviors. In this study, a direct shear box and Long Bar Drop Impact (LBDI) apparatus were utilized to examine the dynamic joint shear behavior of artificially jointed rocks. Various dynamic loadings and initial normal stresses under constant normal stiffness (CNS) were considered in the experiment. The experimental results revealed that the dynamic joint shear strength depended on the initial normal stress and joint roughness.

Keywords: Long bar drop impact (LBDI) apparatus, Direct shear box, Constant Normal Stiffness (CNS) condition, Dynamic joint shear behavior, Artificial jointed specimen.

1 INTRODUCTION

Underground rock structures under high-stress conditions are exposed to potential fault-slip, rock ejection, and rock fall hazards caused by the discontinuities. For that reason, the underground structure has been designed based on the shear behavior of rock discontinuities acquired from the rock joint shear test. However, most mechanical properties related to the design of underground rock structures have been obtained under static or quasi-static loading conditions, even though rock structures are often subjected to dynamic loading sources, such as seismic waves, blast loading, and percussion drilling. Recent research has shown that the dynamic behavior of the mechanical properties of rocks, including the uniaxial compressive strength (Xia et al. 2008; Dai et al. 2010; and Zhou et al., 2017), tensile strength (Dai et al. 2010; Dai et al. 2008; Wang. 2009), and fracture toughness (Backers et al. 2003; Oh et al. 2019), may differ from their behavior under static or quasi-static loading conditions. Thus, the joint shear behavior may also exhibit different behaviors under dynamic loading conditions.

Previous studies (Kim 2023; Yao et al. 2021; Wang et al. 2021), have conducted dynamic joint shear testing using the Hopkinson bar (HB) system, which is commonly used to investigate the dynamic fracture behavior of rock and rock-like materials. To examine the dynamic shear behavior of a joint, however, the HB system's short-wavelength stress waves may be inadequate. Consequently, a new dynamic loading system is necessary.

In this study, we present a novel dynamic joint shear testing system that applies stress waves with long wavelengths to the rock joint under constant normal stiffness (CNS) conditions. We perform dynamic joint shear experiments on an artificial rock specimen under various initial normal stress and dynamic loading conditions. Our results demonstrate that the dynamic joint shear behavior is significantly influenced by the initial normal stress conditions. We compare and discuss our experimental results with numerical analysis results to clarify joint shear behavior.

2 EXPERIMENTAL SETUP

2.1 Sample preparation

Gypsum was used to make artificial with artificial roughness, which were produced using a mixture of a 450:139 weight ratio of plaster and water and a mold with artificial roughness. The mold was created using a 3-D rough joint model generated through a random midpoint displacement method based on the fractional Brownian profile method (Seo & Um 2012). The joint roughness was quantified using the joint roughness coefficient (JRC), which was controlled using the standard deviation (σ) and Hurst exponent (H). The 3D-printed mold was produced by Cubicon's single Plus-320 3-D printer (precision x and y axes: 6.25; z-axis: 1.25), with the 3D printer model generated using Cubicreator V software. The physical and mechanical properties of the specimens, such as density, elastic modulus, Poisson's ratio, uniaxial compressive strength, and tensile strength, were 1630 kg/m3, 5.63 GPa, 0.11, 29 MPa, and 3 MPa, respectively. An image of a specimen is shown in Fig. 1.

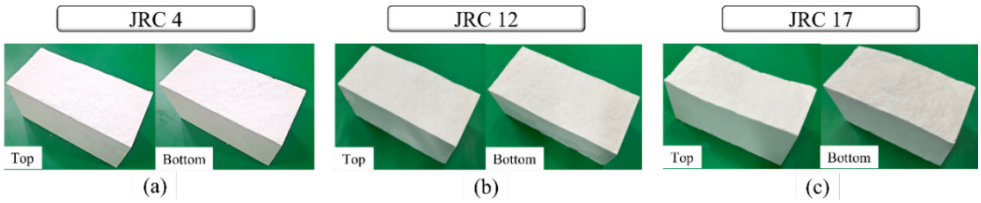

Figure 1. Photographs of three pairs of artificial rock joint specimens with different JRCs: (a) JRC 4, (b) JRC 12, and (c) JRC 17.

2.2 Dynamic shear loading test system

The dynamic shear loading test system, which includes the long bar drop impact (LBDI) apparatus and the CNS direct shear box, has been prepared to perform the dynamic joint shear experiment under CNS conditions.

Figure. 2 compares stress wave propagation between the SHPB system and the LBDI system. The blue and red stress waves represent compression and tension, respectively. In the SHPB system (see Fig. 2(a)), a short impact bar collides with a long incident bar and generates a stress wave with a short wavelength. When this wave reaches the specimen interface, part of it is reflected, and the remaining wave propagates towards the specimen. The wave then reaches the end of the specimen and is perfectly reflected, causing tension, and possibly resulting in spallation (tensile fracture) if the net tensile stress exceeds the specimen's tensile strength.

On the other hand, in the LBDI system, the long impact bar contacts the short incident bar, causing the propagation of a long wavelength stress wave to the specimen. Spallation is less likely to occur because the net stress in the specimen is unlikely to exceed its strength due to the combination of the

input wave and reflected wave (as shown in Fig. 2(b)). Based on the concept mentioned above, the LBDI apparatus is designed as presented in Fig. 3(a).

The LBDI apparatus consists of three components: the frame, the impact bar, and the incident bar. When the impact bar is dropped from a predetermined height onto the incident bar, the specimen is subjected to stress waves generated by the impact. The frame is designed to control the position of the impact bar and constrain its lateral displacement to ensure accurate contact between the impact bar and the incident bar.

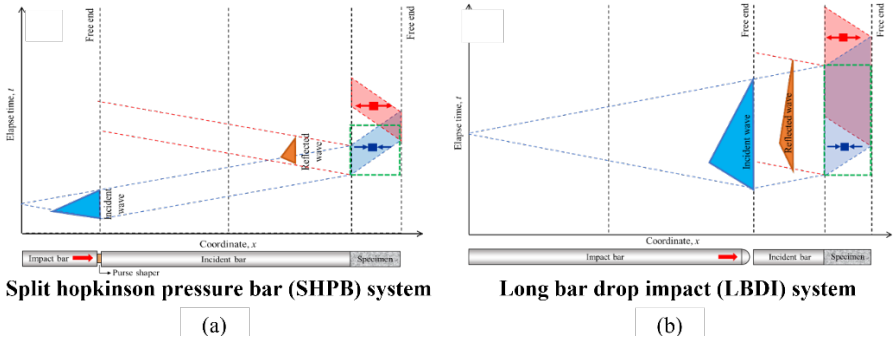

Figure 2. Bar impact-induced stress wave interaction on the specimen in (a) SHPB and (b) LBDI system

Secondly, the CNS direct shear box in the dynamic shear loading system is designed to apply dynamic joint shearing and achieve constant normal stiffness in specimens, as shown in Fig. 3(b). A circular bushing is installed on the top of the shear box to control the lateral movement of the incident bar. The joint shear specimen is placed in the shear box, and the top specimen is moved downward by the stress wave from the incident bar. The load cell for measuring the shear load is placed at the base of the lower specimen, while the load cell for measuring the normal stress due to normal dilation is placed on the side. An accelerometer is attached to the top specimen center to measure the acceleration of the specimen center during the movement along the shear direction. The displacement of the specimen center also be acquired by double integrating the measured acceleration.

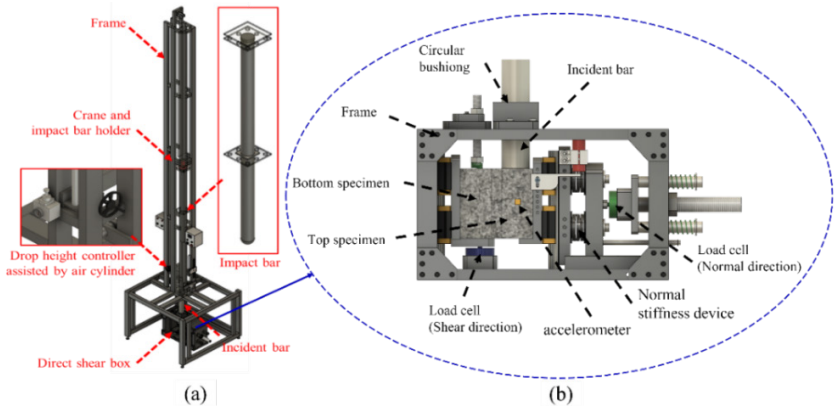

Figure 3. Schematic design of dynamic joint shear test system (a) LBDI apparatus and (b) CNS direct shear box.

2.3 Experimental condition

This study investigated the influence of the initial normal stress and joint roughness coefficient (JRC) on dynamic joint shear behavior. The LBDI apparatus drop height was controlled at 0.6 m, 0.8 m, and 1.0 m to apply various dynamic loading conditions. The roughness of the artificial joint was varied as JRC = 4, 12, and 17 to examine the effect of the roughness on the joint shear behavior. The initial normal stress was also changed to 0.5 and 1.0 MPa, respectively. The normal stiffness of the spring was maintained at 5 kN/mm.

3 RESULTS

3.1 Measurement of dynamic shear stress, normal stress, and displacements

Figure 4(a) illustrates the measured shear stress-time histograms for various JRCs and initial normal stresses. The wave lengths of shear stresses are approximately 0.8 milliseconds, and the peak shear stress increases with increasing JRC for a given initial normal stress. Additionally, the increase in initial normal stress causes an increase in peak shear stress. Figure 4(b) depicts the normal stress-time history curve under various JRC and initial normal stress conditions. As with the shear stress-time histogram, the magnitude of the normal stress is proportional to the JRC and the initial normal stress. In addition, the shape of the normal stress curve has the same history as the shape of the shear stress curve. For JRC 4, the first peak shear stress is 0.68 MPa and 1.03 MPa for initial normal stress conditions of 0.5 MPa and 1.0 MPa, respectively. For JRC 12, the first peak shear stress is 0.98 MPa and 1.71 MPa under the same conditions, and for JRC 17, it is 2.54 MPa and 3.72 MPa for the same conditions.

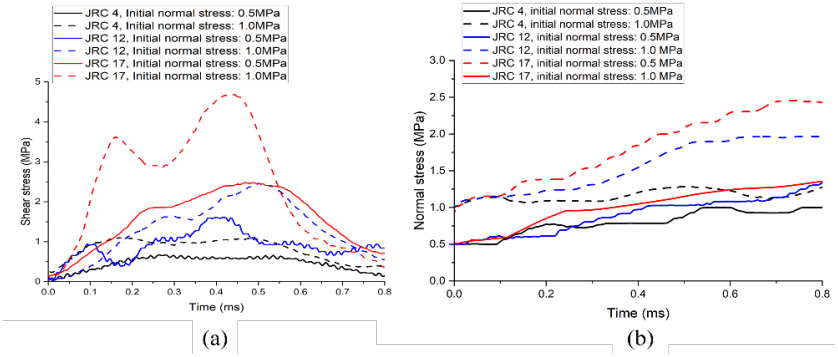

Figure 4. Shear stress and normal stress-time curves with different JRC and initial normal stress (a) shear stress and (b) normal stress.

Figure 5(a) represents the shear stress-shear displacement curves for different JRCs and initial normal stresses. The first peak shear stresses corresponding to the shear strength appear before 0.1 mm shear displacement. The shear stress-shear displacement curve of the specimen for JRC 17 and 1 MPa initial normal stress shows the typical curve which appears at the static shear loading test. Figure 5(b) shows the shear stress-normal stress histories of 5kN/mm stiffness joint specimens with different JRCs for 0.5 MPa and 1 MPa initial stress. The shear-normal stress curves are shown to be on a continuous line when the joint roughness is the same, and the shear failure criterion is able to be suggested by connecting the peak shear stress values with a straight line.

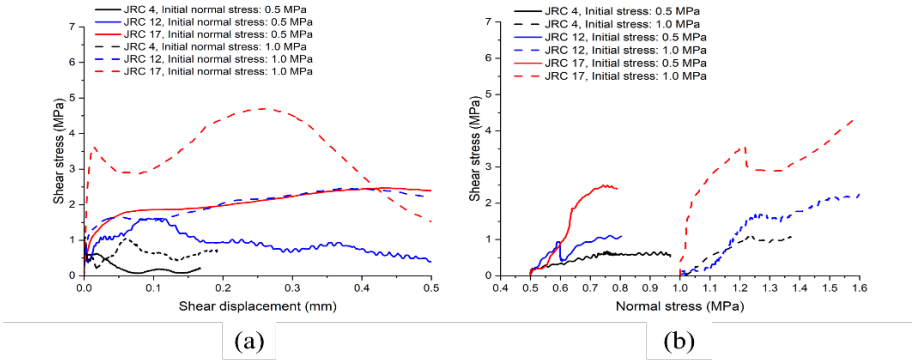

Figure 5. Shear stress-shear displacement and shear stress-normal stress curves with different JRC and initial normal stress (a) Shear stress-shear displacement (b) Shear stress - normal stress.

3.2 Observation of dynamic joint shear behavior using DIC

Figure. 6 shows the snapshots captured by a high-speed camera and the results of digital image correlation (DIC) analysis near the first peak shear stress during dynamic joint shear behavior. The results of the DIC analysis for various boundary conditions support the hypothesis that the shear stress decreases after the initial maximum value. Overall, the x and xy strains indicate that the joint is displaced in the shear direction while undergoing uniform straining across the entire specimen. In addition, the results of the x, y, and xy strain analyses indicate that the normal shear behavior of the joint continued until the first maximum shear stress was determined without causing local strain concentration and partial failure due to spalling phenomenon.

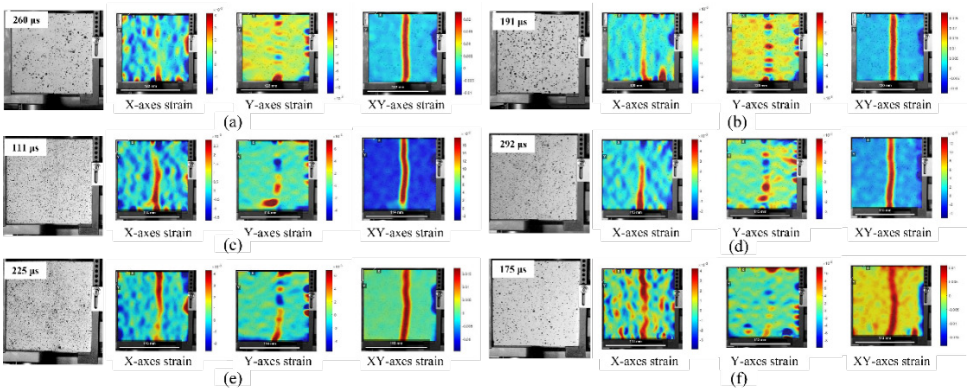

Figure 6. Snapshots of high-speed camera images and DIC results with different JRC and initial normal stress when (a) JRC 4, 0.5MPa (b) JRC 4, 1.0MPa (c) JRC 12, 0.5MPa (d) JRC 12, 1.0MPa (e) JRC 17, 0.5MPa; (f) JRC 17, 1.0MPa

4 COMPARISON WITH NUMERICAL ANALYSIS RESULTS

The 3DEC software was utilized to simulate a dynamic joint shear experiment to examine the influence of loading rate on the shear strength of rock joints under CNS conditions. Dynamic and static simulation applied the CY model (Cundall & Hart 1984) to apply the internal mechanisms of the gradual failure of the joint surface of the shear behavior. The incident waveform applied to the specimen used the actual stress waveform induced by the LBDI apparatus. As boundary conditions, k = 5kN/mm of normal stiffness and σ_n= 0.5MPa and σ_n = 1.0MPa of initial normal stress were chosen. Due to page limitations, only the JRC = 4 case was analyzed and compared to explain the difference between dynamic and static loading on joint shear strength. Figure 7 (b) illustrates the shear strength - initial normal stress under both dynamic and static conditions. The shear strength dependent to the normal stress increment, as well as loading-rate. In addition, the Barton-Bandies (BB) formula (Bandis et al. 1983) and static simulation results were significantly different from the dynamic joint shear experiment results.

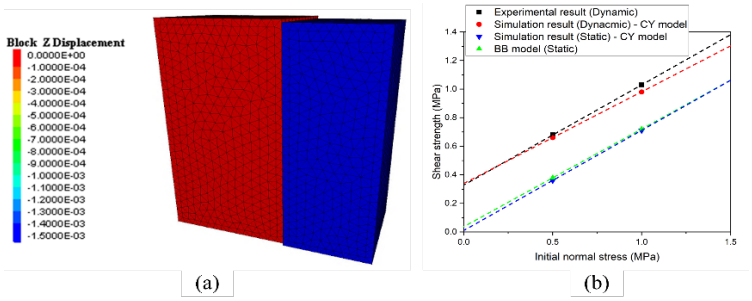

Figure 7. Comparison of experimental and numerical shear strengths (a) 3DEC model and (b) numerical shear strength-initial normal stresses

5 CONCLUSIONS

This study presents the results of dynamic CNS joint shear experiments conducted on artificial joint specimens using an LBDI device. The findings demonstrate that the LBDI apparatus is a suitable tool for examining joint dynamic shear behavior. The experimental results indicated that the shear behavior of the rough joint was influenced by the JRC and initial normal stress conditions. Additionally, the first peak shear stress and the ratio of shear stress to normal stress were found to be significantly influenced by these factors (i.e., JRC and initial normal stress). The joint shear strength depends on the loading condition and the normal stress increase. In addition, there was a significant difference in the joint shear strength between the dynamic and static conditions in both the experimental and numerical analyses. The findings of this study are expected to contribute to the development of optimized design and stability assessment criteria for rock structures subjected to dynamic loads.

ACKNOWLEDGEMENTS

The authors would like to express our sincere appreciation and gratitude to Dr. Bohyun Kim at NIOSH for his invaluable contribution and assistance in this research study. This work was supported by the Agency for Defense Development by the Korean Government (UE201046GD).

REFERENCES

Backers, T., Fardin, N., Dresen, G., & Stephansson, O. 2003. Effect of loading rate on Mode I fracture toughness, roughness and micromechanics of sandstone. *International Journal of Rock Mechanics and Mining Sciences, 40(3)*, 425-433.

Bandis, S. C., Lumsden, A. C., & Barton, N. R. 1983. Fundamentals of rock joint deformation. *In International Journal of Rock Mechanics and Mining Sciences & Geomechanics Abstracts Vol. 20, No. 6,* pp. 249-268. Pergamon.

Cundall, P. A & Hart, R. D. 1984. Analysis of Block Test No. 1: Inelastic Rock Mass Behavior. Characterization of Joint Behavior, *Final Report. Phase 2. Itasca Consulting Group Incorporated*.

Dai, F., Huang, S., Xia, K., & Tan, Z. 2010. Some fundamental issues in dynamic compression and tension tests of rocks using split Hopkinson pressure bar. *Rock mechanics and rock engineering, 43*, 657-666.

Dai, F., Xia, K., & Luo, S. N. 2008. Semicircular bend testing with split Hopkinson pressure bar for measuring dynamic tensile strength of brittle solids. *Review of Scientific Instruments 79(12)*, 123903.

Oh, S. W., Min, G. J., Park, S. W., Kim, M. S., Obara, Y., & Cho, S. H. 2019. Anisotropic influence of fracture toughness on loading rate dependency for granitic rocks. Engineering Fracture Mechanics, 221, 106677.

Seo, H. K & Um, J. G. 2012. Generation of roughness using the random midpoint displacement method and its application to quantification of joint roughness. *Tunnel and Underground Space*, 22(3), 196-204.

Wang, F., Xia, K., Yao, W., Wang, S., Wang, C., & Xiu, Z. 2021. Slip behavior of rough rock discontinuity under high velocity impact: Experiments and models. *International Journal of Rock Mechanics and Mining Sciences 144*, 104831.

Wang, Q. Z., Li, W., & Xie, H. P. 2009. Dynamic split tensile test of flattened Brazilian disc of rock with SHPB setup. *Mechanics of Materials 41(3)*, 252-260.

Xia, K., Nasseri, M. H. B., Mohanty, B., Lu, F., Chen, R., & Luo, S. N. 2008. Effects of microstructures on dynamic compression of Barre granite. *International Journal of Rock Mechanics and Mining Sciences 45(6)*, 879-887.

Kim, G. G. 2023. A study on the construction of dynamic joint shear test apparatus and the evaluation of rock joint shear strength. *Chonbuk National University master's thesis.*

Yao, W., Wang, C., Xia, K., & Zhang, X. 2021. An experimental system to evaluate impact shear failure of rock discontinuities. *Review of Scientific Instruments 92(3)*, 034501.

Zhou, Z. L., Yuan, Z. H. A. O., Jiang, Y. H., Yang, Z. O. U., Xin, C. A. I., & Li, D. Y. 2017. Dynamic behavior of rock during its post failure stage in SHPB tests. *Transactions of Nonferrous Metals Society of China 27(1)*, 184-196.